Integration of an anti-resonant hollow-core fiber with a multimode Yb-doped fiber for high power near-diffraction-limited laser operation

HUIZI LI,[1,3] CHARU GOEL,[2,3] JICHAO ZANG,[2] SIDHARTHAN RAGHURAMAN,[2] SHAOXIANG CHEN,[2] MUHAMMAD ROSDI ABU HASSAN,[2] WONKEUN CHANG,[2] AND SEONGWOO YOO[2,*]

[1] *CNRS -International - NTU - THALES Research Alliances (CINTRA), Nanyang Technological University, 50 Nanyang Drive, 637553, Singapore*

[2] *The Photonics Institute, School of Electrical and Electronic Engineering, Nanyang Technological University, 50 Nanyang Avenue, 639798, Singapore*

[3] *The authors contributed equally to this work*

[*] *seon.yoo@ntu.edu.sg*

Abstract: We proposed and demonstrated mode cleaning in a high-power fiber laser by integrating an anti-resonant hollow-core fiber (AR-HCF) into a multimode laser cavity of an ytterbium (Yb)-doped fiber (YDF). An in-house mode-matched AR-HCF was fusion-spliced to a commercial multimode LMA-YDF, ensuring efficient fundamental mode coupling. The AR-HCF inflicts a high propagation loss selectively on higher-order modes, facilitating fundamental mode operation. Thus, the AR-HCF works as an efficient spatial mode filter embedded in the multimode fiber laser cavity and reinforces preferential amplification of the fundamental mode. Beam quality factor enhancement was achieved from $M^2 = 2.09$ to 1.39 at an output power of 57.7 W (pump-power limited). The beam quality can be further improved by refining the AR-HCF fabrication. The proposed technique has a great potential to be exploited in other multimode fiber laser cavities involving erbium- or thulium-doped fibers and obviates the need for complicated specialty active fiber designs. Compared with the commonly used fiber bending technique, our method can achieve an efficient higher-order mode suppression without inducing mode-field deterioration.

1. Introduction

Hollow core fibers (HCFs) have attracted much research attention in the past decades because of their unique characteristics. Different from conventional solid silica fibers, HCFs confine light in the air hole, leading to high material damage threshold, low optical nonlinearity, and ultra-low waveguide dispersion [1,2]. These outstanding features enable HCFs to be advantageous over conventional solid core fibers for low-loss transmission in the mid-IR region [3], sensing [4], ultrafast pulse compression [5], and supercontinuum generation by gas-filling [6]. Anti-resonant (AR)-HCFs are a new class of HCFs that operate following the anti-resonant reflecting optical waveguide guidance model [7] and inhibited coupling of fundamental core mode with lossy dielectric modes [8]. Compared with the photonic bandgap HCFs, AR-HCFs have multiple broad transmission bands and simplified cladding structure, making the technology more accessible. AR-HCFs are inherently few-moded but all the core modes are leaky in nature, with higher order modes (HOMs) suffering orders of magnitude higher propagation loss than the fundamental mode. Therefore, AR-HCFs can support large mode areas of up to 40 μm core diameter [9,10], while maintaining effective single mode operation. There has been significant research interest in tapping the potential of AR-HCFs in a variety of optical systems, such as high-power laser

beam delivery [11,12], ultra-fast pulse delivery [13,14], wavelength filters [15], and mechanical force sensors [4].

High-power fiber lasers have evolved rapidly and have been investigated extensively over the past decades. They serve important applications in various fields, such as advanced manufacturing, aerospace and energy resource exploration [16]. The major challenge of power scaling in high-power fiber lasers is the occurrence of nonlinear effects, which can significantly degrade laser power scalability [17–19]. Enlarging the mode field area of a step-index fiber and lowing its core numerical aperture (NA) is an efficient way to suppress the nonlinear effects without deteriorating the beam quality [20]. However, lowering core NA encounters practical limitation of ∼0.038 set by the fabrication tolerance [21]. In addition, the low NA undermines the confinement capability of the fiber core, which causes bending induced deteriorations such as beam distortion and high loss in the fundamental mode [22]. Special waveguide designs without the core NA limitation have been proposed [23,24], which have stringent fabrication and limited compatibility with commercial fiber components.

Therefore, a step-index LMA fiber is still the main fiber platform in high power lasers. Instead of complicating the design, post-fabrication fiber-processing methods like fiber bending and tapering are often employed to suppress HOMs [25–29]. 1.36 kW in a near single-mode laser beam ($M^2 = 1.4$) has been achieved with a 12 cm bending radius by diode pumping [25]. Bending however deteriorates mode profile and reduces the mode size, defeating the purpose of LMA fiber [28]. 600 W single transverse mode laser based on tapered double-clad YDF by diode pumping has been demonstrated [27]. However, tapering reduces mechanical strength of the fiber and requires much more precautions when handling. Other techniques of insertion a spatial mode filter in laser cavity include single-mode-multimode-single-mode (SMS) structure, splicing with a SMF28 at the output end, and the method of employing fiber grating were studied [30–32] . However, standard single mode fiber, such as SMF28, has a small core diameter which can easily trigger nonlinear effects at high power. Multimode fiber grating is capable of handling high power beams due to its LMA, but the grating period determines the corresponding wavelength of each mode, saddling the system with precise temperature control system.

Hollow core waveguide (HCW) has been proposed as an external mode filter for quantum cascade lasers (QCLs) [33,34]. But HCWs are hardly to be spliced with the active fiber by current splicing technique, thus require free space coupling. In this work, we proposed and demonstrated an alternative method utilizing the latest AR-HCF technology as a novel spatial mode filter by spliced into a laser cavity to suppress HOMs. The technique of splicing mode-matched AR-HCF to LMA-YDF has been introduced [35]. The AR-HCF in that work acted as an external beam cleaner and the power fraction of HOMs in the laser output was lost to achieve nearly fundamental mode output. Here in this paper, the splicing technique is firstly exploited for integrating AR-HCF inside a laser cavity to reinforce fundamental mode in cavity which is not affected by the loss of HOMs. The laser output beam quality was improved from $M^2 = 2.09$ in the absence of AR-HCF to $M^2 = 1.39$ after the integration of AR-HCF, at 57.7 W lasing power. The demonstration suggests a promising technique for power scalable single mode operation in a high power fiber laser.

2. Hollow-core fiber design and theoretical analysis

The LMA-YDF employed in this work is a commercial double-clad fiber (LMA-YDF-25/250-VIII) from Nufern, having a 25 μm core diameter and 19.8 μm mode field diameter (MFD) for LP_{01} mode at a wavelength of 1065 nm. The cladding diameter is 250 μm and core NA is 0.06. The LMA-YDF can support four LP modes and simulations reveal that LP_{11} mode is expected to dominate the multimode lasing signal in the absence of any spatial mode selection method; the simulation results are elaborated in the next paragraph. To suppress the LP_{11} mode in the cavity, we designed a single-ring, seven tube lattice AR-HCF with a 28 μm core diameter, 18 μm

capillary inner diameter, 250 µm cladding diameter, and 0.78 µm capillary thickness as shown in Fig. 1(a). Its LP_{01} mode has MFD of 20.4 µm MFD. The thickness of capillary walls decides the wavelengths corresponding to the anti-resonant region characterized by low propagation loss in the AR-HCF. Our design ensures that the conventional YDF emission band (1010 nm-1100 nm) lies in the low-loss anti-resonant band. Moreover, the core diameter is chosen to support matching MFD with the LMA-YDF for low splice loss. The ratio of capillary to core diameter is optimized to be = 0.64, so as to achieve resonant coupling of LP_{11} core mode to lossy cladding mode, leading to higher order mode extinction ratio (HOMER) above 1000 [36]. The key parameters of the LMA-YDF and designed AR-HCF are listed in the Table 1. We apply full-vector finite element method using commercial software COMSOL Multiphysics to calculate the mode fields distribution of the first four core modes in the AR-HCF, as shown in Fig. 1(b). The HOMs are subjected to the great losses in the AR-HCF as they propagate along the fiber length, leading to an effective single mode operation. The calculated propagation losses of the LP_{01}, LP_{11}, LP_{21}, and LP_{02} modes at 1065 nm wavelength in the designed AR-HCF are 0.023 dB/m, 25 dB/m, 4.5 dB/m and 12 dB/m respectively.
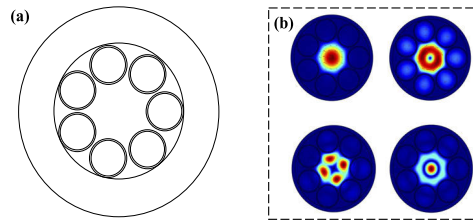

Fig. 1. (a) Cross-section of the designed AR-HCF; (b) Mode field distribution of LP_{01}, LP_{11}, LP_{21} and LP_{02} in the AR-HCF.

Table 1. Fiber parameters of LMA-YDF, designed AR-HCF and fabricated AR-HCF

Fiber parameters	LMA-YDF	Designed ARHCF	Fabricated ARHCF
Core diameter (µm)	25	28	31.3
Outer diameter (µm)	250	250	161.3
MFD (µm)	19.8	20.4	23.6
HOMER	N. A	1087	10.9

We first theoretically investigate effectiveness of our method for beam cleaning in a laser cavity composed of the LMA-YDF and the AR-HCF. Figure 2 shows the simulation results of individual mode growth in the cavity. A reflection of 4%−100% linear cavity under 975 nm pumping is assumed. We used the numerical model given in [37] to investigate modal behaviors when they co-exist in the cavity. When all the supported modes are freely allowed (e.g., neither fiber bending nor AR-HCF in the cavity), the LP_{11} dominates in the cavity as clearly shown in Figs. 2(a) and (b). It is not surprising because the overlap of the LP_{01} with the center of the doped core is high, leading to a rapid growth and saturation while the LP_{11} having a higher overlap at the edge of the core can grow faster than the saturated LP_{01}. Our observation is consistent with previous studies [37]. As shown in Fig. 2(b), the LP_{11} is the dominant mode in the LMA-YDF alone cavity. We note that the LMA-YDF supports four LP modes, but the LP_{02} mode power does not grow due to its poor overlap with the doped area, and no cavity loss other than the outcoupling is assumed.

The high content of HOMs is nearly completely suppressed with the help of AR-HCF as a mode cleaner. In Figs. 2(c) and (d), the AR-HCF is placed in the cavity via splicing to the LMA-YDF. We assume 100% feedback at the output end of the AR-HCF and 4% feedback at the pump coupling end of the LMA-YDF (See Fig. 5(b) for the assumed cavity.). With a 1.45 m-long
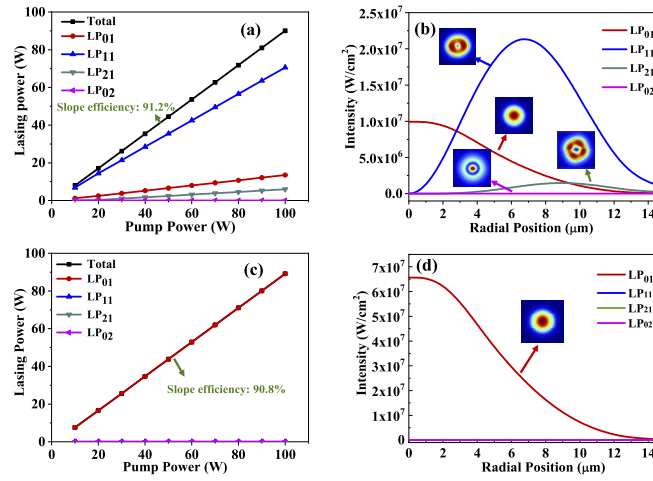
Fig. 2. (a) Simulated lasing output power of the transverse modes versus pump power in the 6 m-long LMA-YDF when kept straight; (b) Intensity of the transverse modes along the radial position of the LMA-YDF at 100 W pump power; (c) Simulated lasing output power of the transverse modes versus pump power with a 1.45 m-long AR-HCF spliced to the LMA-YDF; (d) Intensity of the transverse modes along the radial position of the LMA-YDF at 100 W pump power with the AR-HCF attached.

AR-HCF in the cavity, the LP_{01} mode becomes evidently the dominant mode as presented in Figs. 2(c) and (d). The modal losses are stated in Table 1. The high HOMER of the AR-HCF results in selection of the LP_{01} as the most favorable mode for lasing. The length of the AR-HCF is optimized to efficiently suppress the HOMs, without inducing significant loss to the LP_{01} mode. As shown in Fig. 2(c), all HOMs are completely suppressed with the optimum length of AR-HCF and LP_{01} is the only surviving transverse mode. Consequently, the fundamental mode experiences the lowest loss in the cavity and becomes dominant as re-confirmed in Fig. 2(d). Because of the natural selection of the fundamental mode by the cavity design, the overall efficiency of the laser is not affected by the loss of HOMs (91.2% in Fig. 2(a) versus 90.8% in Fig. 2(c)) unlike in a delivery fiber [11]. By employing the AR-HCF as a part of the laser cavity, LP_{01} mode enjoys preferential gain while the HOMs die out due to the distributed filtering along the AR-HCF.

Bending the YDF is another common way to suppress HOMs in a multimode laser cavity. However, the technique triggers nonlinear effects at high powers, by reducing the effective mode area (A_{eff}) of the YDF [28]. Figure 3(a) shows calculated A_{eff} of LP_{01} mode at 1065 nm in the LMA-YDF for different bending radii. The A_{eff} shows an obvious decrease when the bending radius is smaller than 12.5 cm, which accompanies significant mode profile distortion as shown in the insets. Figure 3(b) shows calculated HOMER (the ratio of the loss of LP_{11} to the loss of LP_{01}) induced by the 12.5 cm bending radius which is the smallest bending radius without inducing noticeable mode distortion. The calculated loss is a combined value of the background loss and bending loss. The HOMER gradually increases from 1010 nm and reaches 2.1 at 1100 nm, but it is too low to achieve sufficient suppression of the HOM. In contrast, the HOMER in AR-HCF is above 1200 over the entire Yb-emission band as shown in Fig. 3(c). The high HOMER and the wavelength insensitive feature clearly highlight the superior performance of AR-HCF as an effective solution to facilitate a fundamental-mode operation in a multimoded fiber cavity over a range of wavelengths.
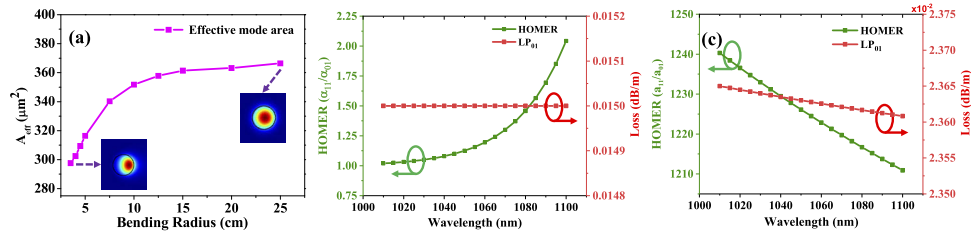
Fig. 3. (a) Calculated A_{eff} of LP_{01} mode at 1065 nm in LMA-YDF-25/250-VIII fiber with different bending radii. (b) Calculated HOMER (α_{11}/α_{01}) (at left Y axis) and calculated loss of LP_{01} mode (at right Y axis) in 12.5 cm radius bent LMA-YDF-25/250-VIII from 1010 nm to 1100 nm. (c) Calculated HOMER(α_{11}/α_{01}) (at left Y axis) and calculated propagation loss of LP_{01} mode (at right Y axis) in designed AR-HCF from 1010 nm to 1100 nm.

3. Experiment results

The AR-HCF was fabricated by the standard stack and draw method. The scanning electron microscopy (SEM) image of the fabricated AR-HCF is shown in Fig. 4(a). The parameters of the fabricated AR-HCF are listed in Table 1. The capillaries have shrunk more than those in the intended design due to insufficient pressurization while fiber is being drawn. As a result, resonant coupling of LP_{11} core mode to dielectric modes is not complete in the fabricated fiber. The propagation losses of the HOMs (LP_{11}, LP_{21} and LP_{02}) at 1065 nm are 1.2 dB/m, 2.5 dB/m, and 14 dB/m respectively, which are lower than the in the original design. In addition, loss in the LP_{01} mode is higher than that in the designed fiber (0.11 dB/m). Thus, a longer AR-HCF was necessary to suppress HOMs at the cost of higher LP_{01} mode loss than in the AR-HCF employed in the simulation (Fig. 2(c)).
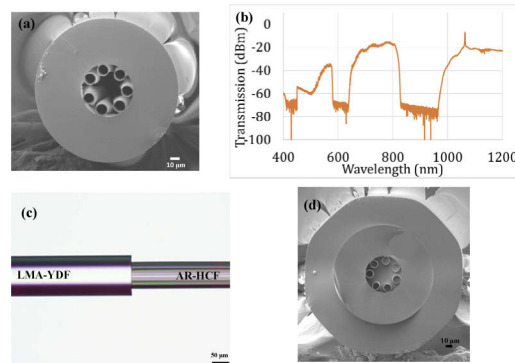
Fig. 4. (a) SEM image of the cross section of the fabricated AR-HCF; (b) Transmission spectrum of the AR-HCF. The peak at ~1060 nm originates from the supercontinuum source used in the measurement; (c) Longitudinal view of spliced section under an optical microscope; (d) SEM image of the cross-section of a broken splice point.

The measured transmission spectrum of the 3 m-long AR-HCF with a supercontinuum source and an optical spectrum analyzer (Yokogawa AQ6373B) is shown in Fig. 4(b); the fiber has a broad transmission band from 1000 nm to 1200 nm which covers entirely the Yb-emission band. The AR-HCF were cleaved using *Fujikura CT-106* with a cleaving angle of 0.2°–0.3°. The LMA-YDF and AR-HCF were spliced by a commercial CO_2 laser-based glass processing station *Fujikura LZM 100*, using an in-house recipe [35]. Figures 4(c) and (d) show the optical microscope image of the longitudinal view of the splice section and SEM image of the transverse
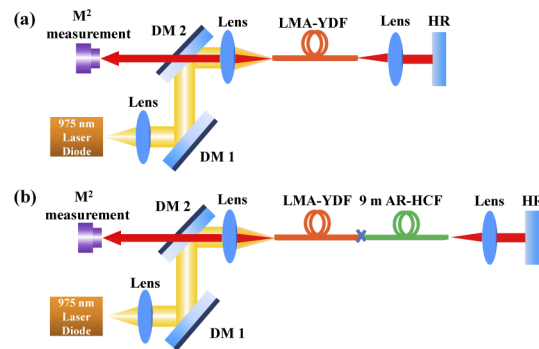
Fig. 5. Configuration of 1065 nm fiber laser based on 6 m multimode LMA-YDF in loose condition (a) without AR-HCF in cavity; and (b) with 9 m AR-HCF integrated into the cavity.

cross-section of the broken splice point, respectively, confirming that the fine structure in the AR-HCF is well-preserved after splicing. The coupling loss of fundamental mode from LMA-YDF to AR-HCF is 0.4 dB and the Fresnel reflection at the glass air interface is expected to be 3.3%. Since the experiment configuration is a 4%−100% linear cavity with the high reflection mirror, the Fresnel reflection at the interface is negligible.

To investigate the performance of the AR-HCF as a spatial mode filter, we established a 1065 nm laser cavity employing 6 m-long LMA-YDF loosely bent at >50 cm bending radius to prevent fiber bending-induced HOMs suppression. The configuration of the fiber laser cavity is shown in Fig. 5(a). The LMA-YDF was cladding pumped by a 975 nm laser diode with pigtailed fiber (105 /125 µm) output. Dichroic mirrors DM1 and DM2 were used for directing the pump light into the LMA-YDF and outcoupling the generated 1065 nm laser signal for characterization, such as the beam quality measurement and power measurement. The 6 m-long Yb-doped fiber is sufficient for ∼99% of pump power absorption. The output signal is sent back into the laser cavity by a high reflection mirror (HR) after a lens. The pump end facet of the fiber was flat cleaved to form 4% feedback. In a separate set of measurements, a 9 m-long AR-HCF was incorporated in the laser cavity as shown in Fig. 5(b). The AR-HCF was spliced to the loosely coiled LMA-YDF.

Lasing performances of the two cavities are investigated using a 50 W wavelength stabilized laser diode. Figure 6(a) shows the measured beam quality from the cavity without the AR-HCF. The mean M^2 is measured as 1.97 at the maximum pump power. However, in the cavity containing the AR-HCF, this is improved to 1.30, as shown in Fig. 6(b). The beam quality improvement is visually noticeable in the beam profiles as presented in the insets. These results signify the role of AR-HCF as a spatial mode filter, enabling beam quality enhancement in a multimode LMA-YDF cavity, as expected theoretically in Section 2. Figure 6(c) shows the lasing efficiency of the laser cavities with and without the AR-HCF. The laser cavity without AR-HCF (blue dots) is characterized by a slope efficiency of 88% with respect to the launched pump power. In contrast, the slope efficiency of the cavity with AR-HCF (red dots) is measured as 77%. The reduction of the efficiency (hence, the output power) is attributed to considerable LP_{01} mode loss accumulated during the round trip along the 9 m-long AR-HCF. The propagation loss of LP_{01} mode is higher in the fabricated fiber than the theoretical value (∼0.11 versus 0.023 dB/m), caused by structural asymmetry as found in Fig. 4(a). Moreover, the low HOMER of 11 in the fiber made it necessary to use a long length (9 m) to filter out the HOMs, causing ∼2 dB loss for the LP_{01} mode. Consequently, the loss caused by the fabrication imperfection led to the reduction in the lasing efficiency. We note that the 9 m length was close to the best compromise between the beam quality and laser efficiency. It should be also noted that the temperature at the

splicing point did not rise during the experiments, confirming the natural mode selection via the AR-HCF as a distributed spatial filter, which otherwise would result in a temperature increase at the splicing point due to the HOMs losses. A linear relationship the output power with and without the AR-HCF as shown in Fig. 6(d) reaffirms the loss-driven natural selection of the LP_{01} mode in the cavity with AR-HCF. It is worth noting that fabrication of AR-HCFs with a lower LP_{01} mode loss (~0.075 dB/m) and higher HOMER (~107) is practical [38], which will improve the laser efficiency to the level that is expected in the numerical study. Thus, our experimental results serve as a proof of concept for the role of AR-HCF as a mode cleaner in the laser cavity.
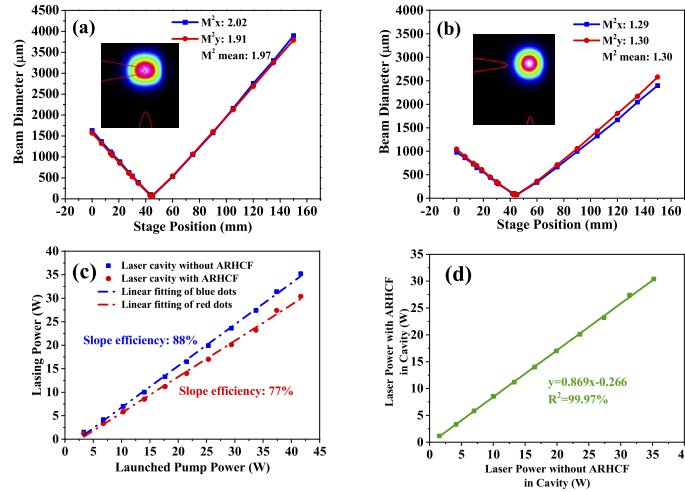
Fig. 6. (a) Measured beam quality and beam profile (insets) at the maximum lasing power (a) cavity without AR-HCF; (b) cavity with AR-HCF integrated inside; (c) Laser output power versus launched pump power, blue dots and blue line represent the cavity without AR-HCF, and red dots and red line represent the cavity with AR-HCF; (d) 1065 nm lasing power from the cavity with AR-HCF versus that from the cavity without AR-HCF.

We investigate the mode selection by the AR-HCF at a higher power level. A 115 W wavelength un-stabilized 975 nm laser diode replaced the wavelength stabilized 50 W pump source in the setup presented in Fig. 5. The same lengths of LMA-YDF and AR-HCF as in Fig. 5 were used in the experiments. Because of the pump wavelength shift, the 6 m long YDF turned out to be not optimum. However, this did not interfere with our comparative study. As presented in Figs. 7(a) and (b), we were able to obtain a beam quality improvement from the mean M^2 value of 2.09 to 1.39 also with the higher power. Linear increase of the output power was also observed as presented in Fig. 7(c). More importantly, Fig. 7(d) shows that the output powers from the two cavities are linear with the same slope as in Fig. 6(d). The consistency in experimental results suggests that the technique can be applied to higher power lasers. The LMA YDF we adopted in this work is a standard fiber (25 μm core diameter) used for kW level lasers. Further scaling in a LMA step-index fiber requires a larger core to mitigate thermal and non-linear limits as studied in [39]. For example, a 60 μm core diameter theoretically can support 10 kW lasing power under a diode pumping configuration [39]. The larger core is unfortunately more liable to higher-order mode excitation. With the advent of larger core AR-HCFs (up to 60–65 μm core diameters [40,41]), we believe that our result provides a feasible approach to reach the theoretical maximum power from a single fiber. It is worth noting that the improved beam quality of 1.39 was limited by deviation of the fabricated AR-HCF from the optimized design. There is a clear prospect of better beam quality improvement.
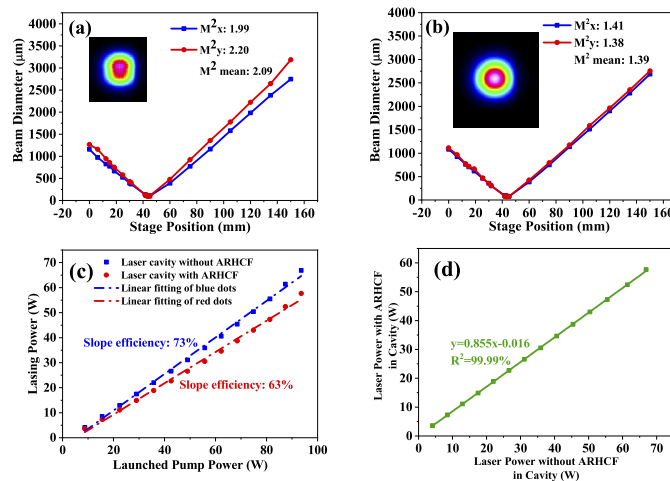
Fig. 7. (a) Measured beam quality and beam profile (insets) at the maximum lasing power (a) cavity without AR-HCF; (b) cavity with AR-HCF integrated inside; (c) Laser output power VS launched pump power, blue dots and blue line represent a laser cavity without AR-HCF, and red dots and red line represent a laser cavity with AR-HCF; (d) 1065 nm lasing power from cavity with AR-HCF VS 1065 nm lasing power from cavity without AR-HCF.

4.   Conclusion

In conclusion, we proposed a method for fundamental mode operation assisted by AR-HCF, which was incorporated in a multimode fiber laser cavity. The AR-HCF works as a mode cleaner, which relies on its inherent high HOMER. The concept of this technique was demonstrated in a multimoded LMA-YDF cavity. A beam quality factor improvement from 2.09 to 1.39 was achieved in a 57.7 W linear laser cavity. Further improvement is achievable by refining fabrication of the AR-HCF. This technique has the potential to be extended to a variety of multimode lasers at any operating spectral band beyond the YDF in a monolithic configuration. It can be a promising solution to maintain near-diffracted-limited laser operation in a high power fiber laser even with the onset of transverse mode instability.

Disclosures. The authors declare no conflicts of interest.

Data availability. Data underlying the results presented in this paper are not publicly available at this time but may be obtained from the authors upon reasonable request.

References

1. F. Poletti, M. N. Petrovich, D. J. Richardson, and M. J. Li, "Hollow-core photonic bandgap fibers: Technology and applications," Nanophotonics **2**(5-6), 315–340 (2013).
2. C. M. Smith, N. Venkataraman, M. T. Gallagher, D. Müller, J. A. West, N. F. Borrelli, D. C. Allan, and K. W. Koch, "Low-loss hollow-core silica/air photonic bandgap fibre," Nature **424**(6949), 657–659 (2003).
3. F. Yu, P. Song, D. Wu, T. Birks, D. Bird, and J. Knight, "Attenuation limit of silica-based hollow-core fiber at mid-IR wavelengths," APL Photonics **4**(8), 080803 (2019).
4. C. Goel, J. Zang, M. Parrot, and S. Yoo, "Temperature-Insensitive Mechanical Sensor Using Multi-Modal Behavior of Antiresonant Hollow-Core Fibers," J. Lightwave Technol. **39**(12), 3998–4005 (2021).
5. M. Gebhardt, C. Gaida, T. Heuermann, F. Stutzki, C. Jauregui, J. Antonio-Lopez, A. Schulzgen, R. Amezcua-Correa, J. Limpert, and A. Tünnermann, "Nonlinear pulse compression to 43 W GW-class few-cycle pulses at 2 μm wavelength," Opt. Lett. **42**(20), 4179–4182 (2017).
6. M. I. Hasan, N. Akhmediev, and W. Chang, "Mid-infrared supercontinuum generation in supercritical xenon-filled hollow-core negative curvature fibers," Opt. Lett. **41**(21), 5122–5125 (2016).
7. F. Yu, M. Xu, and J. C. Knight, "Experimental study of low-loss single-mode performance in anti-resonant hollow-core fibers," Opt. Express **24**(12), 12969–12975 (2016).

8. L. Vincetti and V. Setti, "Waveguiding mechanism in tube lattice fibers," Opt. Express **18**(22), 23133–23146 (2010).

9. L. Provino, "Effect of nested elements on avoided crossing between the higher-order core modes and the air-capillary modes in hollow-core antiresonant optical fibers," Fibers **6**(2), 42 (2018).

10. G. T. Jasion, T. D. Bradley, K. Harrington, H. Sakr, Y. Chen, E. N. Fokoua, I. A. Davidson, A. Taranta, J. R. Hayes, D. J. Richardson, and F. Poletti, "Recent Breakthroughs in Hollow Core Fiber Technology," *2021 Opt. Fiber Commun. Conf. Exhib. OFC 2021 - Proc.* 11309, 1130902-1–1130902-8 (2021).

11. X. Zhu, D. Wu, Y. Wang, F. Yu, Q. Li, Y. Qi, J. Knight, S. Chen, and L. Hu, "Delivery of CW laser power up to 300 watts at 1080 nm by an uncooled low-loss anti-resonant hollow-core fiber," Opt. Express **29**(2), 1492–1501 (2021).

12. W. Huang, X. Ye, Y. Cui, Z. Zhou, Z. Chen, Z. Wang, and J. Chen, "High power laser coupling from solid-core fibers to anti-resonant hollow-core fibers by fiber tapering technology," Proc. SPIE 11849, 118490I (2021).

13. E. Lee, J. Luo, B. Sun, V. Ramalingam, Y. Zhang, Q. Wang, F. Yu, and X. Yu, "Flexible single-mode delivery of a high-power 2 µm pulsed laser using an antiresonant hollow-core fiber," Opt. Lett. **43**(12), 2732–2735 (2018).

14. M. Michieletto, J. K. Lyngsø, C. Jakobsen, J. Laegsgaard, O. Bang, and T. T. Alkeskjold, "Hollow-core fibers for high power pulse delivery," Opt. Express **24**(7), 7103–7119 (2016).

15. X. Huang, K. T. Yong, and S. Yoo, "A method to process hollow-core anti-resonant fibers into fiber filters," Fibers **6**(4), 1–8 (2018).

16. P. Even and D. Pureur, "High-power double-clad fiber lasers: a review," Opt. Devices Fiber Commun. III **4638**, 89 (2002).

17. C. Jauregui, J. Limpert, and A. Tünnermann, "High-power fibre lasers," Nat. Photonics **7**(11), 861–867 (2013).

18. M. N. Zervas and C. A. Codemard, "High power fiber lasers: A Review," IEEE J. Sel. Top. Quantum Electron. **20**(5), 219–241 (2014).

19. D. J. Richardson, J. Nilsson, and W. A. Clarkson, "High power fiber lasers: current status and future perspectives [Invited]," J. Opt. Soc. Am. B **27**(11), B63–B91 (2010).

20. D. Jain and J. K. Sahu, "Large mode area single trench fiber for 2 µm operation," J. Lightwave Technol. **34**(14), 3412–3417 (2016).

21. D. Jain, Y. Jung, P. Barua, S. Alam, and J. K. Sahu, "Demonstration of ultra-low NA rare-earth doped step index fiber for applications in high power fiber lasers," Opt. Express **23**(6), 7407–7415 (2015).

22. F. Kong, K. Saitoh, D. Mcclane, T. Hawkins, P. Foy, G. Gu, and L. Dong, "Mode area scaling with all-solid photonic bandgap fibers," Opt. Express **20**(24), 26363–26372 (2012).

23. A. G. M. C. Swan, C. Liu, D. Guertin, N. Jacobsen, and K. Tankala, "33µm Core Effectively Single-Mode Chirally-Coupled-Core Fiber Laser at 1064-nm," in *Proc. of OFC (2008)* Paper OWU2. (2008).

24. J. M. Fini, "Design of solid and microstructure fibers for suppression of higher-order modes," Opt. Express **13**(9), 3477–3490 (2005).

25. Y. Jeong, J. K. Sahu, D. N. Payne, and J. Nilsson, "Ytterbium-doped large-core fiber laser with 1 kW continuous-wave output power," Opt. Express **12**(25), 6088–6092 (2004).

26. J. P. Koplow, D. A. V. Kliner, and L. Goldberg, "Single-Transverse-Mode Operation of a Coiled Multimode Fiber Amplifier," Opt. Lett. **25**(7), 442–444 (2000).

27. V. Filippov, Y. Chamorovskii, J. Kerttula, A. Kholodkov, and O. G. Okhotnikov, "600 W power scalable single transverse mode tapered double-clad fiber laser," Opt. Express **17**(3), 1203–1214 (2009).

28. J. W. Nicholson, J. M. Fini, A. D. Yablon, P. S. Westbrook, K. Feder, and C. Headley, "Demonstration of bend-induced nonlinearities in large-mode-area fibers," Opt. Lett. **32**(17), 2562–2564 (2007).

29. F. Di Teodoro, J. P. Koplow, S. W. Moore, and D. A. V. Kliner, "Diffraction-limited, 300-kW peak-power pulses from a coiled multimode fiber amplifier," Opt. Lett. **27**(7), 518–520 (2002).

30. J. M. O. Danie, J. S. P. Chan, J. W. Kim, M. Ibsen, J. K. Sahu, and W. A. Clarkson, "Novel technique for mode selection in a large-mode-area fiber laser," Opt. InfoBase Conf. Pap. **19**(13), CWC5 (2010).

31. A. Polynkin, P. Polynkin, A. Schülzgen, M. Mansuripur, and N. Peyghambarian, "Watts-level, short all-fiber laser at 15 µm with a large core and diffraction-limited output via intracavity spatial-mode filtering," Opt. Lett. **30**(4), 403–405 (2005).

32. X. Zhu, A. Schülzgen, H. Li, L. Li, Q. Wang, S. Suzuki, V. L. Temyanko, J. V. Moloney, and N. Peyghambarian, "Single-transverse-mode output from a fiber laser based on multimode interference," Opt. Lett. **33**(9), 908–910 (2008).

33. J. M. Kriesel, G. M. Hagglund, N. Gat, V. Spagnolo, and P. Patimisco, "Spatial mode filtering of mid-infrared (mid-IR) laser beams with hollow core fiber optics," Quantum Sens. Nanophotonic Devices XI **8993**, 899301 (2013).

34. P. Patimisco, A. Sampaolo, M. Giglio, J. M. Kriesel, F. K. Tittel, and V. Spagnolo, "Hollow core waveguide as mid-infrared laser modal beam filter," J. Appl. Phys. **118**(11), 113102 (2015).

35. C. Goel, H. Li, M. R. Abu Hassan, W. Chang, and S. Yoo, "Anti-resonant hollow-core fiber fusion spliced to laser gain fiber for high-power beam delivery," Opt. Lett. **46**(17), 4374–4377 (2021).

36. P. Uebel, M. C. Günendi, M. H. Frosz, G. Ahmed, N. N. Edavalath, J.-M. Ménard, and P. S. J. Russell, "Broadband robustly single-mode hollow-core PCF by resonant filtering of higher-order modes," Opt. Lett. **41**(9), 1961–1964 (2016).

37. M. Gong, Y. Yuan, C. Li, P. Yan, H. Zhang, and S. Liao, "Numerical modeling of transverse mode competition in strongly pumped multimode fiber lasers and amplifiers," Opt. Express **15**(6), 3236–3246 (2007).

38. L. Provino, A. Haboucha, M. Havranek, A. Monteville, D. Landais, O. Le Goffic, X. Insou, M. Barbier, T. Chartier, M. Thual, and T. Taunay, "Large-core hollow-core antiresonant fiber with low-loss and truly single-mode guidance for N-IR wavelengths," *Opt. InfoBase Conf. Pap. Part F121*, 1–2 (2018).

39. J. W. Dawson, M. J. Messerly, R. J. Beach, M. Y. Shverdin, E. A. Stappaerts, A. K. Sridharan, P. H. Pax, J. E. Heebner, C. W. Siders, and C. P. J. Barty, "Analysis of the scalability of diffraction-limited fiber lasers and amplifiers to high average power," Opt. Express **16**(17), 13240–13266 (2008).

40. D. Dobrakowski, A. Rampur, G. Stępniewski, D. Pysz, L. Zhao, Y. Stepanenko, R. Buczyński, and M. Klimczak, "Femtosecond pulse delivery around 1560 nm in large-core anti-resonant fibers," J. Opt. Soc. Am. B **11456**, 1145607-1 (2020).

41. B. Debord, M. Alharbi, T. Bradley, C. Fourcade-Dutin, Y. Y. Wang, L. Vincetti, F. Gérôme, and F. Benabid, "Hypocycloid-shaped hollow-core photonic crystal fiber Part I: Arc curvature effect on confinement loss," Opt. Express **21**(23), 28597–28608 (2013).